Chemical Science

Cite this: *Chem. Sci.*, 2012, **3**, 2515

www.rsc.org/chemicalscience

EDGE ARTICLE

Fe, Co, and Ni ions promote the catalytic activity of amorphous molybdenum sulfide films for hydrogen evolution†

Daniel Merki, Heron Vrubel, Lorenzo Rovelli, Stéphane Fierro and Xile Hu*

Received 29th April 2012, Accepted 24th May 2012
DOI: 10.1039/c2sc20539d

Molybdenum sulfide materials have been shown as promising non-precious catalysts for hydrogen evolution. This paper describes the study of the promotional effects of certain transition metal ions on the activity of amorphous MoS_3 films. Ternary metal sulfide films, M–MoS_3 (M = Mn, Fe, Co, Ni, Cu, Zn), have been prepared by cyclic voltammetry of aqueous solutions containing MCl_2 and $(NH_4)_2[MoS_4]$. Whereas the Mn–, Cu–, and Zn–MoS_3 films show similar or only slightly higher catalytic activity as the MoS_3 film, the Fe–, Co–, and Ni–MoS_3 films are significantly more active. The promotional effects of Fe, Co, and Ni ions exist under both acidic and neutral conditions, but the effects are more pronounced under neutral conditions. Up to a 12-fold increase in exchange current density and a 10-fold increase in the current density at an overpotential of 150 mV are observed at pH = 7. It is shown that Fe, Co, and Ni ions promote the growth of the MoS_3 films, resulting a high surface area and a higher catalyst loading. These changes are the main contributors to the enhanced activity at pH = 0. However, at pH = 7, Fe, Co, and Ni ions appear to also increase the intrinsic activity of the MoS_3 film.

1. Introduction

Solar energy is one of the most desirable renewable energy resources owing to its unparalleled capacity.[1] The intermittent nature of solar energy, however, necessitates storage methods. Storing sunlight energy in the form of chemical fuels is attractive because fuels have much higher energy densities than batteries.[2] In this context, sunlight-driven water splitting to make hydrogen and oxygen becomes an important scheme for solar energy conversion and storage.[1–5] Water splitting might be achieved in one step *via* photoelectrochemistry, or in two steps *via* photovoltaics and electrolyzers.

One key step in water splitting is the hydrogen evolution reaction (HER), *i.e.* the reduction of protons to form dihydrogen ($2H^+ + 2e^- \rightarrow H_2$). The reaction has a thermodynamic potential of 0 V *vs.* SHE. However, without a catalyst, a high overpotential (η) is required for the reaction to take place with a significant rate. To lower the overpotential, and hence to improve the energy efficiency, good HER catalysts need to be employed. Under acidic or neutral conditions, platinum metal is the best catalyst. Compared to Ni-based catalysts that are used in commercial alkaline electrolyzers, Pt appears to be more compatible with the conditions envisioned for one-step photoelectrochemical water splitting.[6] While being highly active and giving high current densities at low overpotentials, Pt is scarce and expensive, which could be prohibitive for large scale applications. The limited availability of Pt prompts the search for non-precious HER catalysts.[2,4,7,8] A growing number of heterogeneous catalysts[5,9–12] have been developed.

There is now increasing interest in using molybdenum sulfide materials as HER catalysts.[8,13,14] Bulk MoS_2 crystals were known to be poor HER catalysts,[15] however, nanocrystals of MoS_2 with unsaturated edge sites exhibit excellent catalytic activity.[11,13,16–18] Except in a solvothermal synthesis,[17] the MoS_2 nanocrystals were normally prepared by sulfidization using H_2S, either under ultra-high vacuum or using thermal treatments. The sulfidization temperature was 400–550 °C. These harsh conditions not only resulted in a high cost for the catalysts, but also limited the choices of substrate support. We recently reported the discovery that amorphous molybdenum sulfide (MoS_x, $x = 2$ and 3) films are highly active HER catalysts.[8,12] Whereas the precatalysts could be either MoS_2 or MoS_3, the active catalyst in the film was proposed to be a reduced molybdenum sulfide species, probably amorphous MoS_2.[12] Unlike MoS_2 nanoparticles which are prepared under elevated temperature, pressure, or vacuum, the amorphous MoS_x films can be prepared by simple solution electrochemistry under ambient conditions. As a result, these amorphous materials are easy to make, less costly, and amenable to large scale applications. Shortly after, a solution method to deposit amorphous MoS_3 catalysts on CdSe-seeded CdS nanorods under similarly mild conditions (90 °C),[19] and a method for sulfidization at about 200 °C[18] were reported. We also showed

Laboratory of Inorganic Synthesis and Catalysis, Institute of Chemical Sciences and Engineering, Ecole Polytechnique Fédérale de Lausanne (EPFL), EPFL-ISIC-LSCI, BCH 3305, Lausanne, CH 1015, Switzerland. E-mail: xile.hu@epfl.ch; Fax: +41 216939305; Tel: +41 216939781

† Electronic supplementary information (ESI) available: Additional XPS, SEM, capacitance, and impedance data. See DOI: 10.1039/c2sc20539d

that chemically produced amorphous MoS_3 particles were active HER catalysts.[20] It is noteworthy that some of these MoS_x materials and their analogues have been successfully employed for photocatalytic HER.[19,21]

Here we show that certain transition metal ions, such as Fe, Co, and Ni, can significantly improve the catalytic activity of amorphous MoS_x films when they are incorporated in the latter materials. The catalysts are characterized by XPS, electron microscopy, ICP, and capacitance measurements, and the electrode kinetics are studied by Tafel analysis and electrochemical impedance spectroscopy.

2. Results and discussion

Cobalt promoted amorphous MoS_3 film

We earlier reported that amorphous MoS_x ($x = 2$ and 3) films were deposited on a working electrode, *e.g.* ITO or glassy carbon, when an aqueous solution of $(NH_4)_2[MoS_4]$ was subject to consecutive cyclic voltammetry experiments.[12] The MoS_x films were active HER catalysts. We then observed that a thin film was also deposited from an aqueous solution of $(NH_4)_2[Co(MoS_4)_2]$ (**1**) in a similar electropolymerization procedure. Complex **1** is a well-defined Co complex that was previously made as a nitrogenase model.[22] Analysis by XPS indicated that the film contains Co, Mo, and S (*vide infra*). Thus, complex **1** serves as a molecular precursor for the ternary metal sulfide film. Furthermore, it is possible to use *in situ* prepared **1**, formed immediately upon the mixing of $CoCl_2$ with $(NH_4)_2[MoS_4]$, as the precursor. The ratio of Co to Mo is not limited to 1 : 2 in the deposition bath.

The Co–Mo–S films are active HER catalysts. To identify the optimal ratio of Co to Mo in the deposition bath, a number of films were prepared on a glassy carbon electrode from solutions in which the concentration ratios of $CoCl_2$ to $(NH_4)_2[MoS_4]$ varied between 1 : 200 and 1 : 2. When the ratio exceeded 1 : 2, a precipitation was observed upon mixing of $CoCl_2$ and $(NH_4)_2[MoS_4]$, so no attempt was made to deposit films from such mixtures. Fig. 1 shows the polarization curves of the Co–Mo–S films at pH = 7 and 0. The Co^{2+} ion promotes the catalytic activity of amorphous MoS_3.

The Co–Mo–S film prepared from a solution where the concentration ratio of Co to Mo is 1 : 3 exhibits the highest activity. The promotion is more profound at pH = 7 (Fig. 1, A). The binary MoS_3 film has a current density of 0.1 mA cm^{-2} at $\eta = 176$ mV. The best Co–Mo–S ternary film reaches the same current density at $\eta = 84$ mV, resulting in a 92 mV decrease in overpotential. At $\eta = 200$ mV, the current density of the Co-promoted film (1.04 mA cm^{-2}) is five times of that of the unpromoted film (0.19 mA cm^{-2}). The effect of Co-promotion is less pronounced but still visible at pH = 0. To reach a current density of 1.0 mA cm^{-2}, the unpromoted film requires an overpotential of 170 mV, whereas the best Co–Mo–S film requires an overpotential of 135 mV. At $\eta = 200$ mV, the current density of the best Co–Mo–S film (17.5 mA cm^{-2}) is three times of that of the unpromoted film (5.5 mA cm^{-2}). Even though the optimal ratio of Co to Mo in the deposition bath is 1 : 3, a significant promotional effect is already observed with a small amount of Co (1 : 200) at both pHs.

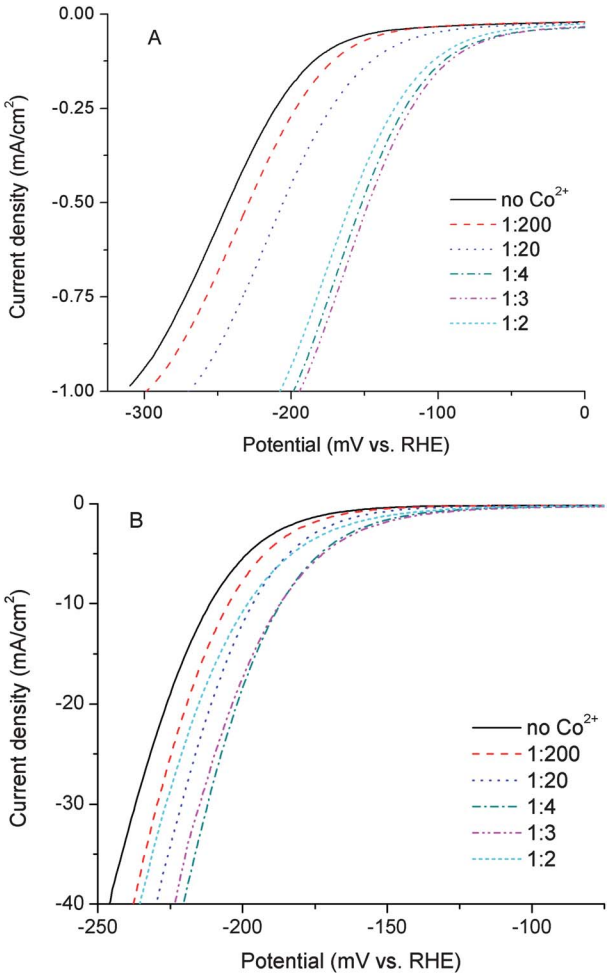

Fig. 1 Polarization curves of unpromoted and Co-promoted MoS_3 films on glassy carbon at pH = 7 (**A**) and pH = 0 (**B**). The Co-promoted films were deposited in solutions with the Co^{2+} to MoS_4^{2-} ratio being between 1 : 200 and 1 : 2. Scan rate: 1 mV s^{-1} (pH = 7) and 5 mV s^{-1} (pH = 0).

The Co–Mo–S film was studied by X-ray photoelectron spectroscopy (XPS). The analysis was performed on a film deposited on FTO, with the optimal Co to Mo ratio of 1 : 3 in the deposition bath. The XPS survey spectrum (Fig. S1 A, ESI†) confirms the presence of cobalt ion in the film. The Co 2p region of the spectrum (Fig. 2, A) shows an intense peak at *ca.* 779 eV and a broad peak at *ca.* 795 eV. These signals are attributed to the transitions from the Co $2p_{3/2}$ and $2p_{1/2}$ orbitals, respectively. A similar spectrum was obtained in a previous XPS study of cobalt sulfide film by Valiuliene *et al.*[23] The Co signals are absent in the XPS spectra of the unpromoted MoS_x films.[12] The S 2p region of the XPS spectrum (Fig. 2 B) exhibits two bands. In addition to the broad and intense band centered around 163 eV, which was also observed in the MoS_x films, a smaller band at *ca.* 169 eV is found. This signal might arise from sulfur atoms interacting with Co ions. Valiuliene *et al.* observed a similar signal and attributed it to cobalt sulfite ($CoSO_3$).[23] The XPS spectrum in the Mo 3d region (Fig. S1 B, ESI†) is very similar to the spectrum of the unpromoted MoS_x films. The two central and more intense peaks are attributed to the transitions from Mo $3d_{3/2}$ and Mo $3d_{5/2}$, respectively. The binding energy indicates a +4 oxidation state for the molybdenum.

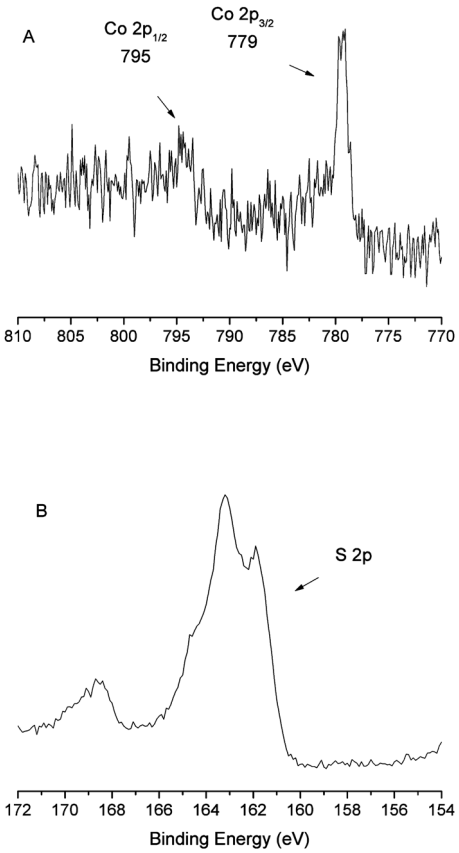

Fig. 2 XPS spectra of the cobalt promoted MoS_3 film on FTO-coated glass; Co 2p region (**A**) and S 2p region (**B**).

We previously showed that a freshly prepared MoS_3 film was reduced to amorphous MoS_2 which was responsible for HER.[12] This was evidenced by the change in the XPS spectra of the film before and after electrolysis. The S 2p spectrum of the MoS_3 film consists of two doublets (Fig. S2 A, ESI†), indicating the presence of both S^{2-} and S_2^{2-} ligands.[20,24] A different XPS spectrum was observed on the film that was subjected to electrolysis at $\eta =$ 200 mV for several minutes. The S 2p spectrum is much narrower (Fig. S2 B, ESI†), and consists of one doublet, similar to the spectrum of MoS_2. To probe whether the same pre-activation process exists for the Co-MoS_3 film, this film was subjected to electrolysis at $\eta = 200$ mV for five minutes. A significant change was observed in the S 2p XPS spectrum of the resulting film (Fig. S3, ESI†). The spectrum is much narrower. While the spectrum could not be fit with one doublet probably due to the presence of some CoS_x species, it suggests that the Co–MoS_3 is activated prior to HER, likely to Co–MoS_2.

We showed earlier that MoS_x films were stable in acidic solutions. The stability of the Co–MoS_3 film was tested in an electrolysis measurement. The catalytic current remained similar during 1 h (Fig. S4, ESI†), indicating a high stability under HER conditions. The film could be oxidized and dissolved at *ca.* 0.7 V *vs.* SHE though (Fig. S5, ESI†).

MoS_3 films promoted with other first-row transition metals

The influence of several other first-row transition metal ions (M^{2+}, M = Mn, Fe, Ni, Cu, Zn) on the HER activity of MoS_3 was also investigated. Since the Co-promoted MoS_3 film showed optimal catalytic activity when the initial M : Mo ratio was about 1 : 3, the initial MCl_2 to $(NH_4)_2[MoS_4]$ ratio was set to this ratio in the deposition bath. The catalytic activities of these ternary M–MoS_3 films towards HER were measured using linear sweep voltammetry (Fig. 3 A and B). Fe^{2+} appears to significantly promote the activity of MoS_3 film at both acidic and neutral pHs, and Ni^{2+} has a pronounced promotional effect at pH = 7. The other ions have a much smaller or no influence on the activity.

Comparison of the promotional effects of different metal ions

Fig. 4 shows the current densities of MoS_3 and M–MoS_3 films (M = Mn, Fe, Co, Ni, Cu, and Zn) at $\eta = 150$ mV and 200 mV. It appears that Fe, Co and Ni ions are all effective promoters. At pH = 7, the best promoter is Co^{2+}, which gives amorphous MoS_3 film a five fold increase in the current density (1.05 mA cm^{-2} *vs.* 0.19 mA cm^{-2}) at $\eta = 200$ mV. At pH = 0, the best promoter is Fe^{2+}, which gives MoS_3 a two fold increase of activity at both $\eta =$ 200 mV and $\eta = 150$ mV (24.9 mA cm^{-2} *vs.* 13.6 mA cm^{-2} and 1.55 mA cm^{-2} *vs.* 0.81 mA cm^{-2}). On the other hand, Mn, Cu, and Zn ions give no or only a small promotion to the activity of MoS_3 films.

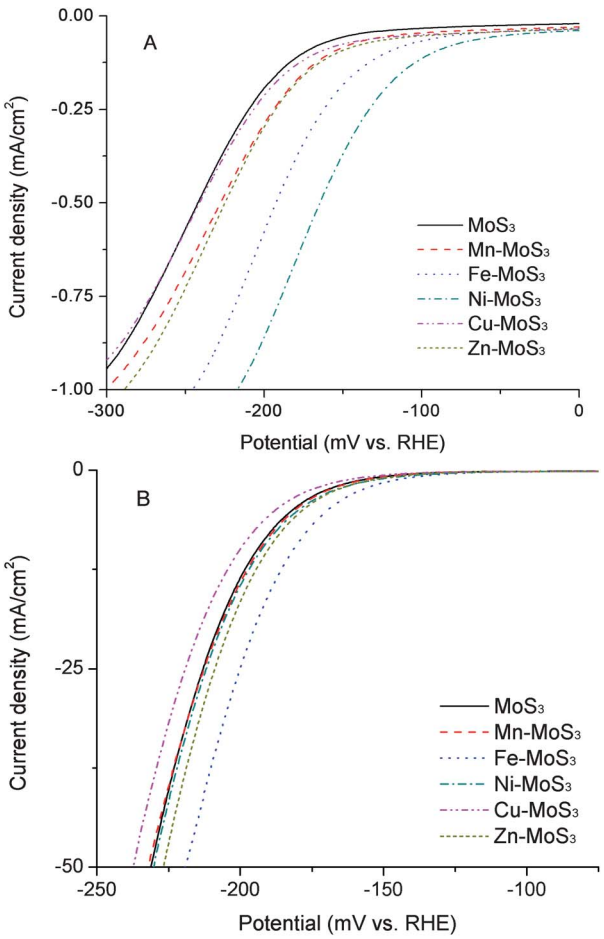

Fig. 3 Polarization curves of unpromoted and M-promoted (M = Mn, Fe, Ni, Cu or Zn) MoS_3 films on glassy carbon at pH = 7 (**A**) and pH = 0 (**B**). The M-promoted films were deposited in aqueous solutions of M^{2+} (0.67 mM) and MoS_4^{2-} (2 mM). Scan rate: 1 mV s^{-1}.

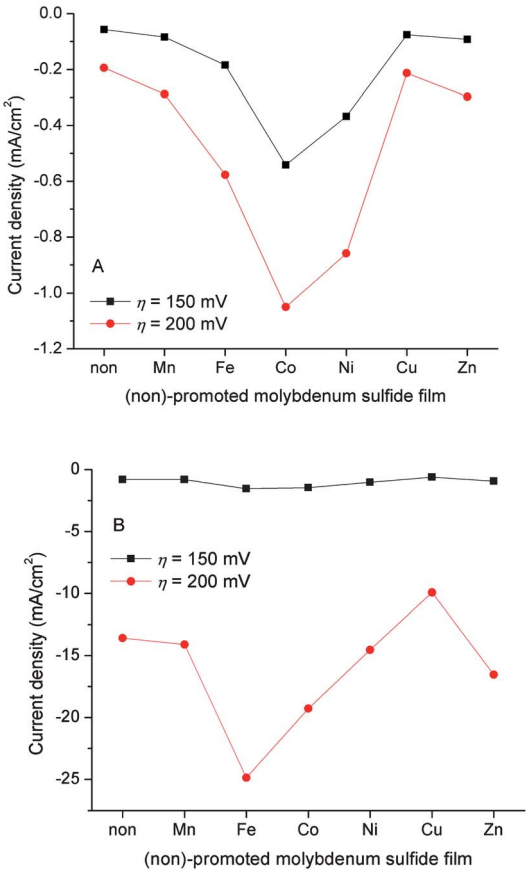

Fig. 4 Current densities of unpromoted and M-promoted (M = Mn, Fe, Co, Ni, Cu or Zn) MoS_3 films on glassy carbon in pH = 7 (**A**) and pH = 0 (**B**) at 150 mV and 200 mV overpotential. The M promoted films were deposited in aqueous solutions of M^{2+} (0.67 mM) and MoS_4^{2-} (2 mM). The current densities were extracted from the respective polarization curves.

Tafel analysis and HER mechanism

Tafel analysis was carried out on the polarization curves of MoS_3 and M–MoS_3 films measured at pH = 0. The results are summarized in Table 1. The Tafel slopes were all found to be between 39–43 mV dec^{-1}. The best three promoters, Fe, Ni and Co, significantly increase the exchange current densities (J_0). The Co–MoS_3 film has the highest J_0 (5.0×10^{-4} mA cm^{-2}), which is a four fold increase from MoS_3. Since this film yields a slightly higher Tafel slope, the current densities at higher overpotentials (*e.g.*, $\eta = 200$ mV) are slightly lower than those of the Fe–MoS_3 film (Fig. 4). Mn, Cu, and Zn, on the other hand, do not bring much change to J_0 or the Tafel slopes, and as a result, their promotional effects are small, if any.

Table 1 Exchange current densities (J_0) and Tafel slopes of unpromoted and M-promoted (M = Mn, Fe, Co, Ni, Cu or Zn) MoS_3 films at pH = 0. The first column gives the overpotential range, where the Tafel analysis was carried out for the respective film

Film	Range of η (mV)	J_0 (mA cm^{-2})	Tafel slope (mV dec^{-1})
MoS_3	151–191	1.2×10^{-4}	39
Mn–MoS_3	152–187	1.1×10^{-4}	39
Fe–MoS_3	140–180	2.0×10^{-4}	39
Co–MoS_3	150–187	5.0×10^{-4}	43
Ni–MoS_3	158–192	2.8×10^{-4}	42
Cu–MoS_3	158–198	1.1×10^{-4}	40
Zn–MoS_3	148–186	1.4×10^{-4}	39

In acidic solutions, hydrogen evolution on a metal surface mainly involves three reactions (eqn (1)–(3)).[25] The common first step is the discharge reaction (1), which is followed by either combination or ion + atom reaction to give H_2. Tafel analysis has been used to distinguish different mechanistic pathways. Assuming a small surface coverage of hydrogen, a fast discharge reaction (1) followed by a rate-determining combination reaction (2) results in a theoretical Tafel slope of 29 mV dec^{-1} at 25 °C (2.303RT/2F). This value is found experimentally for Pt. When (1) is fast and is followed by a slow ion + atom reaction (3), the Tafel slope shall be 38 mV dec^{-1} (2×2.303RT/3F). If (1) is rate-determining or the surface coverage is close to one, the Tafel slope shall be 116 mV dec^{-1} (2×2.303RT/F). Indeed, for many metal electrodes, Tafel slopes of about 29, 38, or 116 mV dec^{-1} have been observed. However, deviations from these values are also common. Many factors may be the origins of the deviation; for example, the surface coverage of hydrogen might be intermediate and potential dependent, or the discharge reaction may have a significant activation barrier.[18,26]

discharge reaction (Volmer step):

$$H_3O^+ + e^- + cat \rightleftharpoons cat\text{–}H + H_2O \quad (1)$$

combination reaction (Tafel step):

$$cat\text{–}H + cat\text{–}H \rightleftharpoons 2\,cat + H_2 \quad (2)$$

ion + atom reaction (Heyrovsky step):

$$H_3O^+ + e^- + cat\text{–}H \rightleftharpoons cat + H_2 + H_2O \quad (3)$$

The correlation between the Tafel slopes and the mechanism of HER was developed for metal surfaces, on which the Volmer step could be observed by cyclic voltammetry. The molybdenum sulfide catalysts are non-metallic, and the Volmer step is not observed by cyclic voltammetry (see Fig. 5, *vide infra*). However, Tafel analysis is still a useful tool here because the experimentally observed Tafel slopes indeed approach a limiting value of 38 mV dec^{-1}. Furthermore, Noskov *et al.* showed earlier by DFT calculations that the hydrogen adsorption step on the edge of MoS_2 was thermally uphill,[13] and therefore it should not be observed at an underpotential as in the case of Pt. Following these considerations, HER catalyzed by amorphous MoS_3 and M–MoS_3 (M = Mn, Fe, Cu, Zn) in acidic solutions seems to occur *via* a fast discharge reaction and then a rate-determining ion + atom reaction. The slightly higher Tafel slopes observed for Co– and Ni–MoS_3 are probably due to a variation in surface coverage of hydrogen rather than a different mechanistic pathway. This hypothesis is supported by the similar electrochemical impedance responses of these films (*vide infra*).

Tafel analysis was carried out on the polarization curves of MoS_3 and M–MoS_3 films measured at pH = 7 as well (Table 2). The Tafel slopes were all found to be between 86 and 96 mV

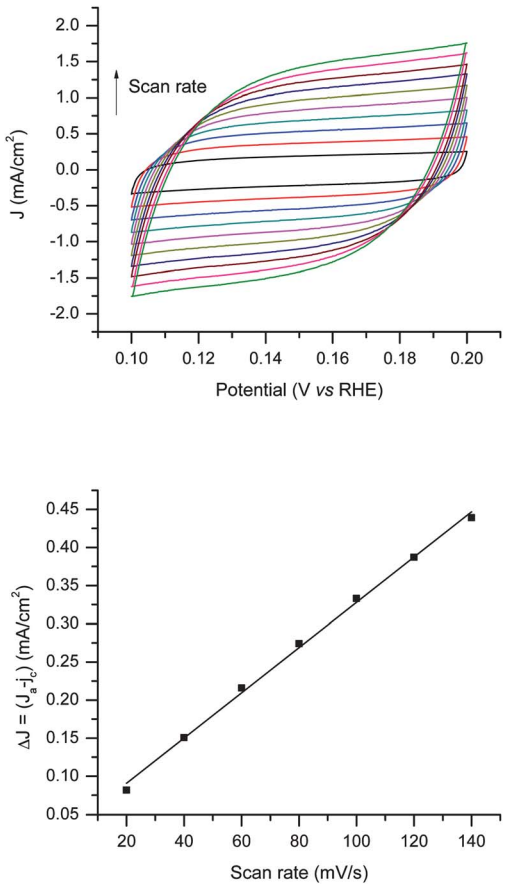

Fig. 5 Cyclic voltammograms at E = 0.1–0.2 V *vs.* RHE (top) and scan-rate dependence of the current density at E = 0.15 V *vs.* RHE (bottom) for the Co–MoS_3 film on FTO in pH = 0.

dec^{-1}. Compared to the unpromoted film, the Fe, Co, and Ni-promoted films again have much larger exchange current densities. The cobalt promotion resulted in a 12 fold increase in J_0. The significant increase in Tafel slopes, from about 38 mV dec^{-1} at pH = 0 to about 90 mV dec^{-1} at pH = 7, indicates a change in the mechanism of hydrogen evolution. We suspect that under the neutral conditions, the rates of the discharge reaction and the ion + atom reaction become comparable, which results in a Tafel slope that is intermediate between 39 and 116 mV dec^{-1}.

Morphology and thickness of M–MoS_3 films

The morphology and thickness of the MoS_3 and M–MoS_3 (M = Mn, Fe, Co, Ni, Cu, Zn) films were studied by scanning electron microscopy (SEM, Fig. S6, ESI†). The incorporation of Fe, Co, or Ni ions resulted in an appreciable change to the morphology of the MoS_3 film, making them more porous. The Mn, Cu and Zn-promoted MoS_3 films, on the other hand, exhibit a similar morphology to the unpromoted MoS_3 film.

The thickness of binary and ternary MoS_3 films was also determined by SEM. The thickness was measured either at the cross-section of the whole electrode assembly (film/FTO/glass), or at places where the film partially peeled off from the FTO coating (see Fig. S7, ESI† for cross-section images of the Co-promoted MoS_3 film). The Co–MoS_3 film is the thickest (400–500 nm), followed by the Fe–MoS_3 (200–300 nm) and Ni–MoS_3 (150–190 nm) films. The unpromoted MoS_3 (100–140 nm), Mn–MoS_3 (100–140 nm), Cu–MoS_3 (100–150 nm), and Zn–MoS_3 (100–130 nm) films have similar thickness. It should be noted that without a promoter such as Fe, Ni, or Co, the maximum thickness for unpromoted MoS_3 film is below 150 nm, regardless the number of scan cycles applied in the electro-deposition.

Table 2 Exchange current densities (J_0) and Tafel slopes of unpromoted and M-promoted (M = Fe, Co, Ni) MoS_3 films at pH = 7[a]

Film	Range of η (mV)	J_0 (mA cm^{-2})	Tafel slope (mV dec^{-1})
MoS_3	171–203	8.9×10^{-4}	86
Fe–MoS_3	137–176	4.8×10^{-3}	95
Co–MoS_3	87–122	1.1×10^{-2}	87
Ni–MoS_3	110–144	1.0×10^{-2}	96

[a] Where the Tafel analysis was carried out for the respective film.

Composition of M–MoS_3 films

The above data show that MoS_3, Mn–MoS_3, Cu–MoS_3, and Zn–MoS_3 films have similar morphology, thickness, and activity. This might originate from a lack of promotional effects of Mn, Cu, and Zn ions, or it could be simply due to the fact that these metal ions are not incorporated into the MoS_3 films. To verify the latter hypothesis, the ratios of M : Mo were probed using XPS (Table 3). Indeed, only 1–5% of Mn, Cu, and Zn ions are present in the respective M–MoS_3 films. On the other hand, the ratios of M : Mo are between 1 : 3 and 1 : 4 for the Fe–, Co–, and Ni–MoS_3 films. These results indicate that the electropolymerization procedures are not efficient in incorporating Mn, Cu, and Zn ions. It was shown earlier that $[M(MoS_4)_2]^{2-}$ complexes were formed by reactions of MCl_2 with $[MoS_4]^{2-}$ only when M = Fe, Co, and Ni, but not when M = Mn, Cu or Zn.[22] The formation of $[M(MoS_4)_2]^{2-}$ complexes thus appears to be important for the incorporation of M into the MoS_3 films.

In order to determine the bulk composition, the films were dissolved in aqua regia and subjected to ICP-OES measurements. As the films contained very little material, only Fe, Co, and Ni–MoS_3 films could be measured within the detection limit of ICP-OES. The Mo content was about 14 μg cm^{-2} for all these three films (Table 3). While the Mo content of the MoS_3 film could not be measured using this method, earlier work showed that it was about 5 μg cm^{-2} in the thickest film.[8] Therefore, Fe, Co, and Ni

Table 3 The ratios of M : Mo in the M–MoS_3 films; M = Mn, Fe, Co, Ni, Cu, Zn[a]

Film	M : Mo (XPS)	Mo (μg cm^{-2})	M : Mo (ICP)
Mn–MoS_3	1 : 18	—	—
Fe–MoS_3	1 : 3.4	14	1 : 3
Co–MoS_3	1 : 3.4	13	1 : 4
Ni–MoS_3	1 : 4	14	1 : 6
Cu–MoS_3	1 : 49	—	—
Zn–MoS_3	1 : 83	—	—

[a] The M–MoS_3 films were prepared from solutions where the concentration ratios of MCl_2 to $(NH_4)_2[MoS_4]$ were 1 : 3.

ions appeared to promote the growth of the MoS_3 film. The M : Mo ratios determined from ICP-OES data are only slightly different from those from the XPS measurement, again indicating the incorporation of a significant amount of Fe, Co, and Ni ions.

Capacitance measurements

The capacitance of the double layer C_{dl} can be used to estimate the effective surface area (A_{eff}) of the solid–liquid interface, assuming that the two quantities are linearly proportional. Cyclic voltammetry can be used as a simple method to determine the C_{dl}.[27] Thus, CV measurements were carried out on MoS_3, Fe–MoS_3, Co–MoS_3, and Ni–MoS_3 films, in the region of 0.1–0.2 V *vs.* RHE, where the currents are mostly due to the charging of the double layer. The capacitance of the films can be calculated from the scan rate dependence of charging current density at E = 0.15 V *vs.* RHE, where the slope of the ΔJ *vs.* scan rate curve is twice the C_{dl}.[27] Fig. 5 shows the CV responses and scan rate dependence of current densities for the Co–MoS_3 film. Those of the MoS_3, Fe–MoS_3, and Ni–MoS_3 films can be found in Fig. S8–S10 (ESI†). Table 4 lists the capacitance values for the four films.

The area-averaged capacitance depends on the electrode materials. It is about 20 μF/cm^2 for a mercury electrode at the point of zero charge,[28] and up to 50 μF/cm^2 for carbon materials.[29] Due to the similarity of MoS_3 and M–MoS_3 electrodes, the area-averaged capacitance of these electrodes should be similar. This value is not known, so the effective surface area of these electrodes could not be calculated. However, the relative surface areas of these films could be estimated by comparing their overall C_{dl} (Table 4). It appears that the Ni–MoS_3 film is slightly rougher, and the Fe–MoS_3 and Co–MoS_3 films have an area that is about three times of that of the MoS_3 film. It is interesting to note that the relative surface areas do not correlate with the amount of Mo in the films (compare Tables 3 and 4).

Electrochemical impedance spectroscopy study

Electrochemical impedance spectroscopy[10,30] (EIS) study is a useful tool to study the electrode kinetics in HER. EIS was carried out on unpromoted and M-promoted (M = Fe, Co, Ni) MoS_3 films. Fig. 6 shows the Nyquist and Bode plots of the EIS response of the Co–MoS_3 film at various overpotentials at pH = 0. The plots for MoS_3, Fe–, and Ni–MoS_3 films are shown in Fig. S11 (ESI†). In the Nyquist plots of all these films, semicircles were observed at higher overpotentials (η > 100 mV). Only one semicircle is observed in each Nyquist plot, indicating that the equivalent circuit for the electrocatalysis is characterized by one time constant. Thus, there is one unit of resistor and capacitor in parallel. The absence of Warburg impedance indicates that mass-transport is rapid enough so that the reaction is kinetically controlled. The dependence of the phase angle ϕ on the frequency (Bode plot) suggests an additional resistor element in series with the above-mentioned two elements. The similarity among the response of all films suggests a similar mechanism for hydrogen evolution (see also section Tafel Analysis).

Thus, the catalytic system is described by a simple equivalent electrical circuit shown in Fig. 7 A. The EIS data were fitted with this circuit model using the program EIS Spectrum Analyzer.[31] Fig. 7 B shows the experimental data and the fitted curve from the EIS response of the Co–MoS_3 film at η = 150 mV. The resistance element R_1 is attributed to the uncompensated solution resistance R_s. The resistance element R_2 is attributed to the charge transfer resistance R_{ct}. The fitting includes a constant-phase element (CPE) which represents the double-layer capacitance under HER conditions C^*_{dl}. The impedance of a CPE is $Z_{CPE} = Q(j\omega)^{-n}$, where Q is a constant representative for the CPE (with the unit of F^{-1} s^{1-n}), j is the imaginary unit, ω is the frequency, and n is a dimensionless parameter that has a value between zero and unity.[32,33] If n equals unity, the CPE behaves as an ideal capacitor. In the present case, n is smaller than 1, indicating that the C^*_{dl} does not behave as an ideal capacitor. Brug

Table 4 The double layer capacitance and the relative surface areas of the MoS_3 and M–MoS_3 films

Film	C_{dl} (μF/cm^2)	Relative surface areas
MoS_3	2300	1.0
Fe–MoS_3	7000	3.0
Co–MoS_3	7600	3.3
Ni–MoS_3	3300	1.4

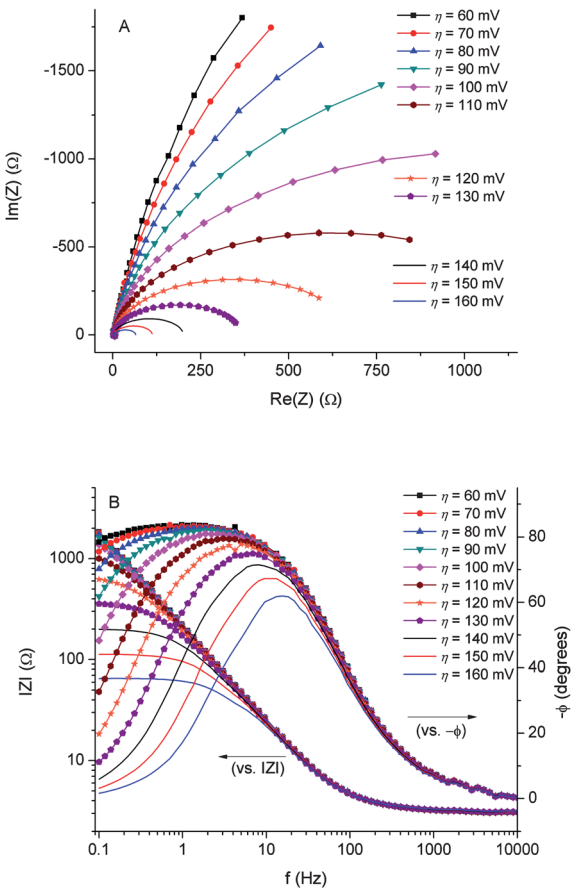

Fig. 6 Nyquist (**A**) and Bode (**B**) plots showing EIS responses of a Co-promoted MoS_3 film on glassy carbon at various HER overpotentials at pH = 0.

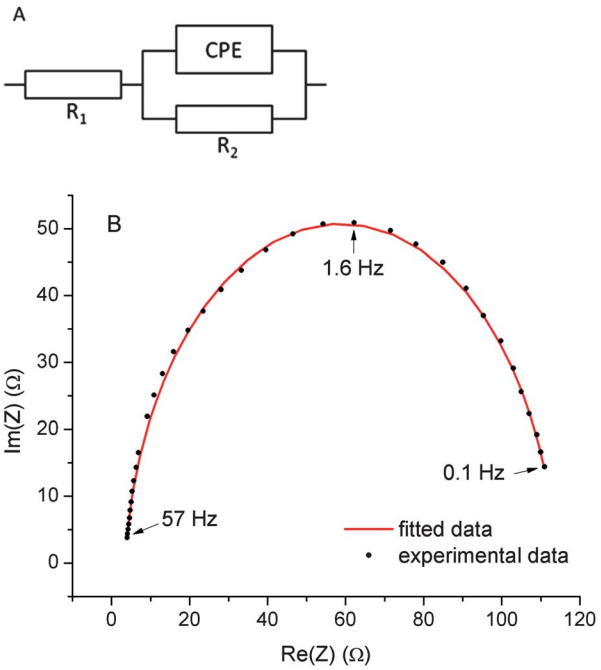

Fig. 7 (**A**) Electrical equivalent circuit used to model the system of all films investigated with EIS. (**B**) Nyquist plot showing the EIS response of Co-promoted MoS_3 film on glassy carbon at $\eta = 150$ mV and pH = 0. The black dots are experimental data and the red line is the fitted curve.

et al. proposed that this type of non-ideality arises from uneven charging of the double layer due to microscopic surface roughness.[32] The parameter n is lower than 1 when the electrode surface is not perfectly flat, but relatively rough. Tables S1–S4 (ESI†) list the values for R_s, R_{ct}, Q^{-1} and n for unpromoted and M-promoted MoS_3 films (M = Fe, Co, Ni).

With values between 3 and 4 Ω, the uncompensated solution resistance R_s is low for all films (Table 5). As expected, this resistance is overpotential independent. The charge transfer resistance R_{ct} is related to the kinetics of electrocatalysis, and a lower value corresponds to a faster reaction rate. R_{ct} depends strongly on overpotential (Fig. 8). At $\eta = 60$ mV, R_{ct} is higher than 15 000 Ω for all catalysts. However, R_{ct} decreases remarkably at higher overpotentials. At $\eta = 160$ mV, R_{ct} falls below 150 Ω for all catalysts (Table 5).

The capacitance C^*_{dl} is obtained using the relation $C^*_{dl} = [Q^{-1}\cdot(R_s^{-1} + R_{ct}^{-1})^{n-1}]^{1/n}$.[32] The calculated values for C^*_{dl} are listed in Tables S1–S4 (ESI†). The C^*_{dl} values determined from EIS are all bigger than the C_{dl} values determined from CV. This is an indication that the C^*_{dl} contains contributions from pseudo-capacitance, probably arising from the adsorption of hydrogen on the surface.[29] The EIS data were also fitted using an electrical equivalent circuit with an ideal capacitor instead of a CPE. Fig. S12 (ESI†) shows the experimental data and the fitted curve from the EIS response of the Co–MoS_3 film at $\eta = 150$ mV. Table S5 (ESI†) lists the values for R_s, R_{ct}, and C^*_{ideal} (double-layer capacitance, using an ideal capacitor) for the same film. As expected, the capacitance C^*_{ideal} is slightly higher than C^*_{dl}.[32]

Hypothesis on the origin of the promotional effects of Fe, Co, and Ni ions

SEM, capacitance, and EIS data indicate a significant composition and morphological change when Fe, Co, or Ni is incorporated into the amorphous MoS_3 film. Clearly, Fe, Co, and Ni ions promote the growth of the MoS_3 film, increasing its surface area and catalyst loading. These changes correlate positively with the enhanced catalytic HER activity. The question is then whether these changes are the sole contributors to the improvement in activity. The intrinsic activity of this series of catalysts is perhaps best described by their exchange current densities (J_0). Table 6 compares the relative exchange current densities with the relative catalyst loadings and surface areas. There is a poor correlation between the relative amount of Mo and the activity, especially among the promoted films. The Fe, Co, and Ni-promoted films have similar content in Mo, but they have different activity. There is also no clear correlation between the relative surface areas and the activity. Nevertheless, the data in Table 6 show that at pH = 0, the increase in HER activity is in

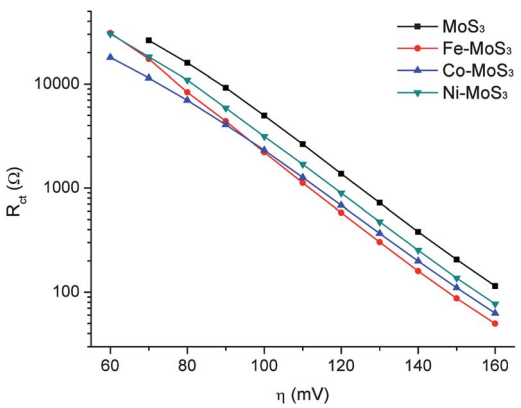

Fig. 8 Dependence of charge transfer resistance R_{ct} on the overpotential for M-promoted MoS_3 films (M = Fe, Co, Ni). The values for R_{ct} were extracted from EIS measurements in pH = 0.

Table 5 Solution resistances (R_s), charge transfer resistances (R_{ct}) at overpotentials of 60 mV and 160 mV, and capacitance of unpromoted and M-promoted MoS_3 films (M = Fe, Co, Ni)[a]

Film	R_s (Ω)	R_{ct} at $\eta = 60$ mV (Ω)	R_{ct} at $\eta = 160$ mV (Ω)	C^*_{dl} (μF/cm²)
MoS_3	3.35 ± 0.07	3.67×10^4	114	3200 ± 200
Fe–MoS_3	3.74 ± 0.15	3.08×10^4	49.8	11 000 ± 600
Co–MoS_3	3.58 ± 0.11	1.80×10^4	62.6	8700 ± 500
Ni–MoS_3	3.45 ± 0.14	3.03×10^4	76.9	7200 ± 400

[a] The resistances and capacitances were obtained by fitting the EIS responses.

the same magnitude as the increase in surface area or catalyst loading. At pH = 7, however, the increase in the activity is significantly higher than the increase in either surface area or catalyst loading. Under these conditions, Fe, Co, and Ni ions seem to increase the intrinsic activity of MoS_3.

Similar promotional effects have been found for the hydrodesulfurization (HDS) reaction of natural gas and refined petroleum products,[34] where the activity of MoS_2 particles is promoted by Co.[35,36] The origin of the promotion is illustrated in Fig. 9, using crystalline MoS_2 as a model catalyst.[35,37] Bulk MoS_2 crystals are hexagonal, and exhibit two types of edge sites: Mo $(10\bar{1}0)$ and S $(\bar{1}010)$ edges. The Mo-edges are partially covered by absorbed sulfur atoms, and are the catalytically active sites. The sulfur edges are not catalytically active. Unpromoted MoS_2 nanocrystals have the shape of truncated triangles, and the predominating edges are the Mo-edges. Nevertheless, S-edges are still present. In Co-promoted MoS_2 nanocrystals, the incorporation of Co ions leads to a hexagonal morphology. The Co ions are located at the S-edges, and the Co-binding S-edges are now catalytically active. As a result, there are more active sites in the Co-promoted MoS_2 nanocrystals, and these catalysts therefore are more active. In other words, the incorporation of Co ions changes both the morphology of MoS_2 crystals (from truncated triangle to hexagonal) and the intrinsic activity of MoS_2 (turning catalytically inactive sites S-edges into active Co-binding S-edges). The promotional effect of Co on MoS_2 nanocrystals was also observed in HER.[16] DFT calculations were employed to validate the hypothesis shown in Fig. 9.[16] The Gibbs free energy of adsorbed atomic hydrogen, ΔG_H, was used as the descriptor for the catalytic efficiency in HER. A smaller absolute value of ΔG_H, close to zero, shall result in a higher activity, *e.g.* higher exchange current density. For MoS_2 crystals, the DFT-calculated ΔG_H is 0.08 eV for the Mo-edge, and 0.18 eV for S edge.[13,16] Thus, HER occurs predominately at the Mo-edge. Incorporation of Co does not affect ΔG_H for the Mo-edge, but lowers the ΔG_H for the S-edge to 0.10 eV.[16] The DFT results suggest that the model in Fig. 9 is also valid for HER catalysts.

The MoS_3 and M–MoS_3 films described here are amorphous, not crystalline. However, the origin of the promotional effects of Fe, Ni and Co ions might be analogous to that of crystalline MoS_2. There are "defect sites" in the amorphous materials. These sites can be considered as unsaturated Mo and S sites where HER may take place. The presence of certain promoter ions can enhance the activity of these unsaturated sites, leading to higher intrinsic activity. This type of promotion is significant at pH = 7, but not at pH = 0. The reason for this is not clear. It might be that at pH = 0, HER catalysis is dominated by the activity of the Mo sites. At pH = 7, however, the activity of the promoted S sites contribute significantly to the overall catalysis.

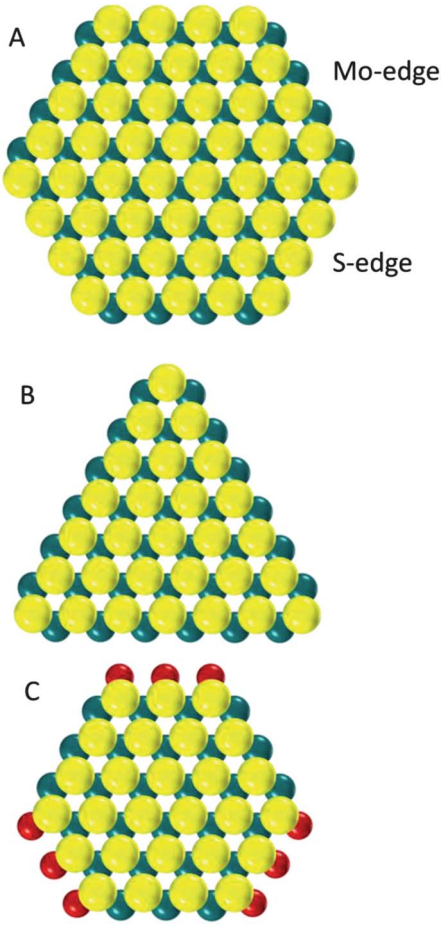

Fig. 9 (**A**) Theoretical hexagonal structure of bulk MoS_2 crystals. (**B**) Truncated triangular structure of unpromoted MoS_2 nanocrystals. (**C**) Hexagonal structure of promoted (Co or Ni) MoS_2 nanocrystals. The Mo-edge sites and the Co sites are partially saturated with sulfur atoms (not shown in the model). Sulfur atoms are in yellow, molybdenum in dark cyan and promoter atoms in red.

3. Conclusions

In summary, amorphous ternary molybdenum sulfide films, M–MoS_3 (M = Mn, Fe, Co, Ni, Cu, Zn), have been prepared by a simple electrochemical method under ambient conditions. A significant amount of Fe^{2+}, Co^{2+}, and Ni^{2+} ions, but only a small

Table 6 Relative exchange current densities at pH = 0 and pH = 7 and relative surface areas of unpromoted and M-promoted MoS_3 films (M = Fe, Co, Ni)[a]

Film	Relative J_0 at pH = 0	Relative J_0 at pH = 7	Relative surface areas	Relative amount of Mo
MoS_3	1.0	1.0	1.0	1.0
Fe–MoS_3	1.7	5.4	3.0	2.8
Co–MoS_3	4.2	12.3	3.3	2.6
Ni–MoS_3	2.3	11.4	1.4	2.8

[a] The values for unpromoted MoS_3 were taken as unity.

amount of Mn^{2+}, Cu^{2+}, or Zn^{2+} ions, could be incorporated into the MoS_3 films. The Fe–, Ni–, and Co–MoS_3 films exhibit significantly higher HER activity than the previously reported unpromoted MoS_3 film. The Mn–, Cu–, and Zn–MoS_3 films, on the other hand, show similar or slightly higher activity to the MoS_3 film. The most active ternary catalysts were prepared from solutions where the concentration ratios of MCl_2 and $(NH_4)_2[MoS_4]$ were 1 : 3. The promotional effects exist under both neutral and acidic conditions. Judging from exchange current density, the promotional effect has the order of Co > Ni > Fe. At pH = 0, the increase in exchange current density is 4.1, 2.3, and 1.7 fold, respectively, compared to unpromoted MoS_3. However, the increase of the current density at a given overpotential (*e.g.* 150 or 200 mV) is attenuated due to larger Tafel slopes for Co– and Ni–MoS_3 films. Practically speaking, the most active catalyst at pH = 0 is Fe–MoS_3 at both η = 150 mV (1.9 fold increase over MoS_3) and η = 200 mV (1.8 fold increase over MoS_3). At pH = 7, a more significant promotional effect of Fe, Co, and Ni ions are found. The most active catalyst at pH = 7 is Co–MoS_3, which is 9.6 fold more active at η = 150 mV and 5.4 fold more active at η = 200 mV than unpromoted MoS_3.

SEM, XPS, ICP-OES, and capacitance studies show that the Fe, Co, and Ni ions promote the growth of the MoS_3 film, increasing its surface area and catalyst loading. These morphological and composition changes result in an enhanced HER catalytic activity. At pH = 0, these changes are the main contributors to the promotional effects of Fe, Co, and Ni ions. At pH = 7, the increase in catalyst loading or effective surface area is not enough to account for the increase in the catalytic activity. Under these conditions, the Fe, Co and Ni ions also increase the intrinsic catalytic activity of MoS_3. It is possible that these metal ions interact with unsaturated sulfur atoms in MoS_3, thereby enhancing its activity toward HER.

Due to their amorphous nature, the M–MoS_3 films contain many defect sites, which may out-number the available edge sites in well-defined MoS_2 nanocrystals. As a result, the amorphous films exhibit higher activity than crystalline nanoparticles. For example, according to polarization measurements, the Co–MoS_3 film gives a current density of *ca.* 18 mA cm^{-2} at η = 200 mV and pH = 0. The corresponding Co–MoS_2 nanoparticles on carbon give a current density of *ca.* 1 mA cm^{-2} at η = 300 mV and pH = 0.[16] Thanks to their ease of synthesis, low cost, and high activity, the promoted amorphous MoS_3 films and their analogues appear to be promising HER catalysts for photoelectrochemical water splitting. This application is being investigated in our lab.

4. Experimental section

Chemicals and reagents

All manipulations were carried out under an inert N_2(g) atmosphere using glovebox techniques unless otherwise mentioned. Iron(II) chloride was prepared by dissolving pure iron metal in a solution of 4.0 M HCl under nitrogen. The excess acid was removed by vacuum and the solid was transferred and stored in a glovebox. Unless noted, all other reagents were purchased from commercial sources and used without further purification.

Physical methods

SEM secondary electron (SE) images were taken on a Philips (FEI) XLF-30 FEG scanning electron microscope. The distances in SEM images were measured with the program ImageJ.[38] Electrochemical measurements were recorded by an IviumStat electrochemical analyzer. A three-electrode configuration was used. For polarization and EIS measurements, a platinum wire was used as the auxiliary electrode and an Ag/AgCl (KCl saturated) electrode was used as the reference electrode. The reference electrode was placed in a position very close to the working electrode with the aid of a Luggin tube. As shown previously, platinum contamination of the working electrode can be ruled out.[8,12] 1.0 M H_2SO_4 (pH = 0) or a standard phosphate buffer from Metrohm (pH = 7), respectively, were used as electrolyte solutions. Double layer capacitance of the films was obtained by cyclic voltammetry experiments in the potential range of 0.100 to 0.200 V *vs.* RHE in 1.0 M H_2SO_4. Scan rates from 20 to 200 mV s^{-1} were chosen. The total current obtained from the addition of the absolute values in the cathodic and anodic wave at 0.150 V *vs.* RHE was plot against the scan rate. The slope of the curve obtained is twice the value of the double layer capacitance. The parameters of the EIS experiments were fixed for all measurements: 100 points were recorded in the frequency range between 0.1 and 10^6 Hz (14 points per decade) with the amplitude of the sinusoidal perturbation fixed at 30 mV. Potentials from −50 to −250 mV *vs.* RHE were applied, with steps of 10 mV. A pretreatment was performed at 0 V *vs.* RHE for 20 s before each experiment and an equilibration time of 5 s was set at the respective potential in order to stabilize the system before the measurement. Experimental EIS data were analyzed and fitted with the software EIS Spectrum Analyzer.[31] The values obtained at the frequency 11.23 Hz were not integrated in the Bode plots, because they deviated largely, probably due to an electronic error. For Tafel analysis, polarization curves were measured at pH = 0 with a scan rate of 1 mV s^{-1}. Auxiliary, reference electrode and working electrode were in the same compartment. The logarithm of the absolute current density of the resulting polarization curve was plotted as a function of overpotential. Tafel analysis was made on the portion of data that showed linear behavior. Therefore, the range of overpotential taken for Tafel analysis varied slightly between different samples. In case of electrochemical film deposition, a fresh titanium wire was used as the auxiliary electrode and an Ag/AgCl (NaCl saturated) electrode was used as the reference electrode. Potentials were referenced to reversible hydrogen electrode (RHE) by adding a value of (0.197 + 0.059 pH) V. The polarization curves measured under one atmosphere of H_2 are nearly identical to those collected in the absence of external H_2, indicating that the potentials measured in the latter experiments are close to the thermodynamically-calibrated values. X-Ray photoelectron spectroscopy (XPS) data were collected by Axis Ultra (Kratos analytical, Manchester, UK) under ultra-high vacuum conditions (<10^{-8} Torr), using a monochromatic Al K_α X-ray source (1486.6 eV), in the Surface Analysis Laboratory of CIME at EPFL. The source power was maintained at 150 W (10 mA, 15kV). Gold (Au $4f_{7/2}$) and copper (Cu $2p_{3/2}$) lines at 84.0 and 932.6 eV, respectively, were used for calibration, and the adventitious carbon 1s peak at 285 eV as an internal standard to compensate for any charging

effects. For quantification, relative sensitivity factors from the supplier were used. ICP-OES analysis was performed with an Optima 2000 spectrometer (Perkin-Elmer). The metal contents were determined using the intensity of the following emission lines: Mo - 203.845; Fe - 239.562; Co - 238.892; Ni - 221.648. Metal standards TraceCERT were purchased from Aldrich and were used for calibration.

Film deposition

The films were deposited on two different types of electrodes: FTO-coated glass plates 15 Ω/sq) and glassy carbon disk electrodes (*ALS*). The glassy carbon disk electrodes were polished with two different Alpha alumina powder (1.0 and 0.3 micron from *CH Instruments*) suspended in distilled water on a Nylon polishing pad (*CH Instruments*) and with Gamma alumina powder (0.05 micron from *CH Instruments*) suspended in distilled water on a Microcloth polishing pad (*CH Instruments*). Before going to the next smaller powder size and at the end of polishing, the electrodes were thoroughly rinsed with distilled water. FTO-coated glass was cut down to rectangular plates of 9 × 25 mm. The plates were thoroughly cleaned and washed with ethanol. An adhesive tape with a hole of 5 mm diameter was attached on each plate in such a way that a circle of 5 mm diameter in the bottom part and a small strip at the top of the plate remained uncovered. The film will be deposited in the area of the circle only and the uncovered strip serves as electrical contact.

In a typical procedure, 2 mL of an aqueous solution of MCl_2 (2.67 mM; M = Mn, Fe, Co, Ni, Cu or Zn) in 0.1 M $NaClO_4$ was added dropwise and under stirring to 6 mL of an aqueous solution of $(NH_4)_2MoS_4$ (2.67 mM) in 0.1 M $NaClO_4$. This was done directly in the electrochemical cell with the auxiliary and the reference electrode already in place. After immersing the working electrode into the resulting solution, twenty five consecutive cyclic voltammetric scans were carried out. The cyclic voltammetry was performed between +0.1 and −1.0 V *vs.* Ag/AgCl (sat. NaCl) and a scan rate of 0.05 V s^{-1} was employed. Finally, the modified electrode was rinsed with distilled water. In the case of the unpromoted molybdenum sulfide film, 2 mL of aqueous 0.1 M $NaClO_4$ was added instead of the MCl_2 solution.

Acknowledgements

This work is supported by a starting grant from the European Research Council under the European Community's Seventh Framework Programme (FP7 2007–2013)/ERC Grant agreement n° 257096. We thank Nicolas Xanthopoulos (EPFL) for help with XPS measurements. X. L. Hu thanks Drs Herve Toulhoat and Pascal Raybaud (IFP Energies Nouvelles, France) for insightful suggestions.

Notes and references

1 N. S. Lewis and D. G. Nocera, *Proc. Natl. Acad. Sci. U. S. A.*, 2006, **103**, 15729–15735.
2 T. R. Cook, D. K. Dogutan, S. Y. Reece, Y. Surendranath, T. S. Teets and D. G. Nocera, *Chem. Rev.*, 2010, **110**, 6474–6502.
3 M. Gratzel, *Nature*, 2001, **414**, 338–344.
4 M. G. Walter, E. L. Warren, J. R. McKone, S. W. Boettcher, Q. X. Mi, E. A. Santori and N. S. Lewis, *Chem. Rev.*, 2010, **110**, 6446–6473.
5 S. Y. Reece, J. A. Hamel, K. Sung, T. D. Jarvi, A. J. Esswein, J. J. H. Pijpers and D. G. Nocera, *Science*, 2011, **334**, 645–648.
6 O. Khaselev and J. A. Turner, *Science*, 1998, **280**, 425–427.
7 V. Artero and M. Fontecave, *Coord. Chem. Rev.*, 2005, **249**, 1518–1535.
8 D. Merki and X. L. Hu, *Energy Environ. Sci.*, 2011, **4**, 3878–3888.
9 M. M. Jaksic, *Electrochim. Acta*, 2000, **45**, 4085–4099; A. Le Goff, V. Artero, B. Jousselme, P. D. Tran, N. Guillet, R. Metaye, A. Fihri, S. Palacin and M. Fontecave, *Science*, 2009, **326**, 1384–1387; B. Winther-Jensen, K. Fraser, C. Ong, M. Forsyth and D. R. MacFarlane, *Adv. Mater.*, 2010, **22**, 1727–1730; P. D. Tran, A. Le Goff, H. J. B. Jousselme, N. Guillet, S. Palacin, H. Dau, M. Fontecave and V. Artero, *Angew. Chem., Int. Ed.*, 2011, **50**, 1371–1374; L. A. Berben and J. C. Peters, *Chem. Commun.*, 2010, **46**, 398–400.
10 E. Navarro-Flores, Z. W. Chong and S. Omanovic, *J. Mol. Catal. A: Chem.*, 2005, **226**, 179–197.
11 T. F. Jaramillo, K. P. Jorgensen, J. Bonde, J. H. Nielsen, S. Horch and I. Chorkendorff, *Science*, 2007, **317**, 100–102.
12 D. Merki, S. Fierro, H. Vrubel and X. L. Hu, *Chem. Sci.*, 2011, **2**, 1262–1267.
13 B. Hinnemann, P. G. Moses, J. Bonde, K. P. Jorgensen, J. H. Nielsen, S. Horch, I. Chorkendorff and J. K. Norskov, *J. Am. Chem. Soc.*, 2005, **127**, 5308–5309.
14 A. B. Laursen, S. Kegnoes, S. Dahl and I. Chorkendorff, *Energy Environ. Sci.*, 2012, **5**, 5577–5591; H. I. Karunadasa, E. Montalvo, Y. J. Sun, M. Majda, J. R. Long and C. J. Chang, *Science*, 2012, **335**, 698–702.
15 W. Jaegermann and H. Tributsch, *Prog. Surf. Sci.*, 1988, **29**, 1–167; H. Tributsch and J. C. Bennett, *J. Electroanal. Chem.*, 1977, **81**, 97–111.
16 J. Bonde, P. G. Moses, T. F. Jaramillo, J. K. Norskov and I. Chorkendorff, *Faraday Discuss.*, 2009, **140**, 219–231.
17 Y. G. Li, H. L. Wang, L. M. Xie, Y. Y. Liang, G. S. Hong and H. J. Dai, *J. Am. Chem. Soc.*, 2011, **133**, 7296–7299.
18 Z. B. Chen, D. Cummins, B. N. Reinecke, E. Clark, M. K. Sunkara and T. F. Jaramillo, *Nano Lett.*, 2011, **11**, 4168–4175.
19 M. L. Tang, D. C. Grauer, B. Lassalle-Kaiser, V. K. Yachandra, L. Amirav, J. R. Long, J. Yano and A. P. Alivisatos, *Angew. Chem., Int. Ed.*, 2011, **50**, 10203–10207.
20 H. Vrubel, D. Merki and X. L. Hu, *Energy Environ. Sci.*, 2012, **5**, 6136–6144.
21 X. Zong, H. J. Yan, G. P. Wu, G. J. Ma, F. Y. Wen, L. Wang and C. Li, *J. Am. Chem. Soc.*, 2008, **130**, 7176–7177; X. Zong, Y. Na, F. Y. Wen, G. J. Ma, J. H. Yang, D. G. Wang, Y. Ma, M. Wang, L. Sun and C. Li, *Chem. Commun.*, 2009, 4536–4538; Y. D. Hou, B. L. Abrams, P. C. K. Vesborg, M. E. Bjorketun, K. Herbst, L. Bech, A. M. Setti, C. D. Damsgaard, T. Pedersen, O. Hansen, J. Rossmeisl, S. Dahl, J. K. Norskov and I. Chorkendorff, *Nat. Mater.*, 2011, **10**, 434–438.
22 A. Muller, E. Diemann, R. Jostes and H. Bogge, *Angew. Chem., Int. Ed. Engl.*, 1981, **20**, 934–955.
23 G. Valiuliene, A. Zeliene, V. Jasulaitiene and I. Mozginskiene, *Russ. J. Appl. Chem.*, 2003, **76**, 71–75.
24 Because different kinds of sulfur ligands might have similar binding energies in XPS, it is not possible to assign the two doublets.
25 J. O. M. Bockris and E. C. Potter, *J. Electrochem. Soc.*, 1952, **99**, 169–186.
26 J. G. Thomas, *Trans. Faraday Soc.*, 1961, **57**, 1603–1611.
27 E. Gileadi, *Physical Electrochemistry*, Wiley-VCH, Weinheim, 2011.
28 S. Trasatti and O. A. Petrii, *Pure Appl. Chem.*, 1991, **63**, 711–734.
29 B. E. Conway, V. Birss and J. Wojtowicz, *J. Power Sources*, 1997, **66**, 1–14.
30 A. J. Bard and L. R. Faulkner, *Electrochemical Methods: Fundamentals and Applications*, John Wiley & Sons, Inc., New York, 2001; Gamry Instruments Application Note: Basics of Electrochemical Impedance Spectrocopy. Available at http://www.gmary.com; A. Damian and S. Omanovic, *J. Power Sources*, 2006, **158**, 464–476.
31 A. S. Bondarenko and G. A. Ragoisha, *EIS Spectrum Analyser*, website: www.abc.chemistry.bsu.by/vi/analyser.
32 G. J. Brug, A. L. G. Vandeneeden, M. Sluytersrehbach and J. H. Sluyters, *J. Electroanal. Chem.*, 1984, **176**, 275–295.
33 Brug *et al.* called the dimensionless parameter alpha, where alpha = 1−*n*.

34 R. Prins, V. H. J. Debeer and G. A. Somorjai, *Catal. Rev. Sci. Eng.*, 1989, **31**, 1–41.
35 S. Kasztelan, H. Toulhoat, J. Grimblot and J. P. Bonnelle, *Appl. Catal.*, 1984, **13**, 127–159; L. S. Byskov, J. K. Norskov, B. S. Clausen and H. Topsoe, *J. Catal.*, 1999, **187**, 109–122; P. Raybaud, J. Hafner, G. Kresse, S. Kasztelan and H. Toulhoat, *J. Catal.*, 2000, **190**, 128–143; P. Raybaud, J. Hafner, G. Kresse, S. Kasztelan and H. Toulhoat, *J. Catal.*, 2000, **189**, 129–146; J. V. Lauritsen, S. Helveg, E. Laegsgaard, I. Stensgaard, B. S. Clausen, H. Topsoe and E. Besenbacher, *J. Catal.*, 2001, **197**, 1–5; H. Schweiger, P. Raybaud and H. Toulhoat, *J. Catal.*, 2002, **212**, 33–38; H. Schweiger, P. Raybaud, G. Kresse and H. Toulhoat, *J. Catal.*, 2002, **207**, 76–87; H. Toulhoat and P. Raybaud, *J. Catal.*, 2003, **216**, 63–72; M. Brorson, A. Carlsson and H. Topsoe, *Catal. Today*, 2007, **123**, 31–36; P. Raybaud, *Appl. Catal., A*, 2007, **322**, 76–91; A. D. Gandubert, E. Krebs, C. Legens, D. Costa, D. Guillaume and P. Raybaud, *Catal. Today*, 2008, **130**, 149–159.
36 Y. Okamoto, K. Tamura and T. Kubota, *Chem. Commun.*, 2010, **46**, 2748–2750.
37 L. P. Hansen, Q. M. Ramasse, C. Kisielowski, M. Brorson, E. Johnson, H. Topsoe and S. Helveg, *Angew. Chem., Int. Ed.*, 2011, **50**, 10153–10156; J. V. Lauritsen, M. V. Bollinger, E. Laegsgaard, K. W. Jacobsen, J. K. Norskov, B. S. Clausen, H. Topsoe and F. Besenbacher, *J. Catal.*, 2004, **221**, 510–522; S. Helveg, J. V. Lauritsen, E. Laegsgaard, I. Stensgaard, J. K. Norskov, B. S. Clausen, H. Topsoe and F. Besenbacher, *Phys. Rev. Lett.*, 2000, **84**, 951–954; H. Toulhoat, P. Raybaud, S. Kasztelan, G. Kresse and J. Hafner, *Catal. Today*, 1999, **50**, 629–636.
38 ImageJ 1.44p; Wayne Rasband, National Institutes of Health, USA, http://imagej.nih.gov/ij.